This article was downloaded by: [University of California, Riverside Libraries]
On: 29 October 2014, At: 15:37
Publisher: Taylor & Francis
Informa Ltd Registered in England and Wales Registered Number: 1072954 Registered office: Mortimer House, 37-41 Mortimer Street, London W1T 3JH, UK

Dekker Encyclopedia of Nanoscience and Nanotechnology, Third Edition

Publication details, including instructions for authors and subscription information:
http://www.tandfonline.com/doi/book/10.1081/E-ENN3

Graphene and Graphene Multilayers: Phonon Thermal Transport

Alexander A. Balandin [a], Denis L. Nika [b]

[a] Department of Electrical Engineering and Materials Science and Engineering Program, University of California—Riverside, Riverside, California, U.S.A.

[b] Department of Electrical Engineering and Materials Science and Engineering Program, University of California—Riverside, Riverside, California, U.S.A. E. Pokatilov Laboratory of Physics and Engineering of Nanomaterials, Department of Theoretical Physics, Moldova State University, Chisinau, Moldova

Published online: 10 Jun 2014

To cite this entry: Alexander A. Balandin, Denis L. Nika. Graphene and Graphene Multilayers: Phonon Thermal Transport. *In* Dekker Encyclopedia of Nanoscience and Nanotechnology, Third Edition. Taylor and Francis: New York, Published online: 10 Jun 2014; 1668-1684.

To link to this chapter: http://dx.doi.org/10.1081/E-ENN3-120050110

PLEASE SCROLL DOWN FOR CHAPTER

Full terms and conditions of use: http://www.tandfonline.com/page/terms-and-conditions

This article may be used for research, teaching, and private study purposes. Any substantial or systematic reproduction, redistribution, reselling, loan, sub-licensing, systematic supply, or distribution in any form to anyone is expressly forbidden.

The publisher does not give any warranty express or implied or make any representation that the contents will be complete or accurate or up to date. The accuracy of any instructions, formulae, and drug doses should be independently verified with primary sources. The publisher shall not be liable for any loss, actions, claims, proceedings, demand, or costs or damages whatsoever or howsoever caused arising directly or indirectly in connection with or arising out of the use of this material.

Downloaded by [University of California, Riverside Libraries] at 15:37 29 October 2014

Graphene and Graphene Multilayers: Phonon Thermal Transport

Alexander A. Balandin
Department of Electrical Engineering and Materials Science and Engineering Program, University of California—Riverside, Riverside, California, U.S.A.

Denis L. Nika
Department of Electrical Engineering and Materials Science and Engineering Program, University of California—Riverside, Riverside, California, U.S.A., and E. Pokatilov Laboratory of Physics and Engineering of Nanomaterials, Department of Theoretical Physics, Moldova State University, Chisinau, Moldova

Abstract
In this entry, we review thermal properties of graphene and multilayer graphene and discuss in detail the optothermal Raman technique developed for the thermal conductivity measurements. We also outline different theoretical approaches used for the description of phonon transport in graphene and provide comparison with the available experimental thermal conductivity data.

INTRODUCTION

Heat removal has become a crucial issue for continuing progress in electronic industry owing to increased levels of dissipated power density and speed of electronic circuits.[1] Self-heating is a major problem in optoelectronics and photonics.[2] These facts stimulated recent interest in thermal properties of materials. Acoustic phonons—fast-moving quanta of the crystal lattice vibrations—are the main heat carriers in a variety of material systems. The phonon and thermal properties of nanostructures are substantially different from those of bulk crystals.[3–16] Semiconductor thin films or nanowires do not conduct heat as well as bulk crystals due to increased phonon-boundary scattering[4,5] as well as changes in the phonon dispersion and density of states (DOS).[3–10] However, theoretical studies suggested that phonon transport in strictly two-dimensional (2-D) and one-dimensional (1-D) systems can reveal exotic behavior, leading to infinitely large *intrinsic* thermal conductivity.[11,12] These theoretical results have led to discussions of the validity of Fourier's law in low-dimensional systems[17,18] and further stimulated interest in the acoustic phonon transport in 2-D systems.

In this entry, we focus on the specifics of the acoustic phonon transport in graphene. After a brief summary of the basics of thermal physics in nanostructures and experimental data for graphene's thermal conductivity, we discuss, in more detail, various theoretical approaches to calculation of the phonon thermal conductivity in graphene.

BASICS OF PHONON TRANSPORT AND THERMAL CONDUCTIVITY

The main experimental technique for investigation of the acoustic phonon transport in a given material system is the measurement of its lattice thermal conductivity.[19,20] In this section, we define the main characteristics of heat conduction. The thermal conductivity is introduced through Fourier's law:[21,22]

$$\vec{\phi} = -K\nabla T \tag{1}$$

where $\vec{\phi}$ is the heat flux, ∇T is the temperature gradient, and $K = (K_{\alpha\beta})$ is the thermal conductivity tensor. In isotropic medium, thermal conductivity does not depend on the direction of heat flow and K is treated as a constant. The latter is valid for small temperature variations only. In a wide temperature range, thermal conductivity is a function of temperature, i.e., $K \equiv K(T)$. In general, in solid materials, heat is carried by phonons and electrons so that $K = K_{\mathrm{p}} + K_{\mathrm{e}}$, where K_{p} and K_{e} are the phonon and electron contributions, respectively. In metals or degenerately doped semiconductors, K_{e} is dominant due to the large density of free carriers. The value of K_{e} can be determined from the measurement of the electrical conductivity σ via the Wiedemann–Franz law:[23]

$$\frac{K_{\mathrm{e}}}{\sigma T} = \frac{\pi^2 k_{\mathrm{B}}^2}{3e^2} \tag{2}$$

where k_{B} is Boltzmann's constant and e is the charge of an electron. Phonons are usually the main heat carriers in

Copyright © 2014 by Taylor & Francis. All rights reserved.

Downloaded by [University of California, Riverside Libraries] at 15:37 29 October 2014

carbon materials. Even in graphite, which has metal-like properties,[24] the heat conduction is dominated by acoustic phonons.[25] This fact is explained by the strong covalent sp^2 bonding, resulting in high in-plane phonon group velocities and low crystal lattice unharmonicity for in-plane vibrations.

The phonon thermal conductivity can be written as

$$K_{\mathrm{p}} = \Sigma_j \int C_j(\omega)\upsilon_j(\omega)\upsilon_j(\omega)\tau_j(\omega)d\omega \tag{3}$$

where summation is performed over the phonon polarization branches j, which include two transverse acoustic branches and one longitudinal acoustic branch, υ_j is the projection of the phonon group velocity $\vec{\upsilon}_j = d\omega_j/d\vec{q}$ on the temperature gradient direction for the j^{th} branch, which, in many solids, can be approximated by the sound velocity, τ_j is the phonon relaxation time, $C_j = \hbar\omega_j \partial N_0(\hbar\omega_j/k_{\mathrm{B}}T)/\partial T$ is the contribution to heat capacity from the j^{th} branch, and $N_0\left(\hbar\omega_j/k_{\mathrm{B}}T\right) = \left[\exp(\hbar\omega_j/k_{\mathrm{B}}T) - 1\right]^{-1}$ is the Bose–Einstein phonon equilibrium distribution function. The phonon mean-free path (MFP) Λ is related to the relaxation time through the expression $\Lambda = \tau\upsilon$ (υ is the average phonon group velocity). In the relaxation-time approximation (RTA), various scattering mechanisms, which limit the MFP, are usually considered as additive, i.e., $\tau_j^{-1} = \sum_i \tau_{ij}^{-1}$, where i denotes scattering mechanisms. In typical solids, acoustic phonons, which carry the bulk of heat, are scattered by other phonons, lattice defects, impurities, conduction electrons, and interfaces.[26–29]

In ideal crystals, i.e., crystals without lattice defects or rough boundaries, Λ is limited by the phonon–phonon scattering due to the crystal lattice anharmonicity. In this case, thermal conductivity is referred to as intrinsic. The anharmonic phonon interactions, which lead to finite thermal conductivity in three dimensions, can be described by the Umklapp processes.[26] The Umklapp scattering rates depend on the Grüneisen parameter γ, which determines the degree of the lattice anharmonicity.[26,27] Thermal conductivity is extrinsic when it is mostly limited by extrinsic effects such as phonon-rough boundary or phonon-defect scattering.

In nanostructures, the phonon energy spectra are quantized due to the spatial confinement of the acoustic phonons. The quantization of the phonon energy spectra usually leads to decreasing phonon group velocity. The modification of the phonon energies, group velocities, and DOS, together with phonon scattering from boundaries affect the thermal conductivity of nanostructures. In most of the cases, the spatial confinement of acoustic phonons results in a reduction of the phonon thermal conductivity.[30,31] However, it was predicted that the thermal conductivity of nanostructures embedded within the acoustically hard barrier layers can be increased via the spatial confinement of acoustic phonons.[6,7,10,32]

The phonon-boundary scattering can be evaluated as[29]

$$\frac{1}{\tau_{\mathrm{B},j}} = \frac{\upsilon_j}{D}\frac{1-p}{1+p} \tag{4}$$

where D is the nanostructure or grain size and p is the specularity parameter defined as a probability of specular scattering at the boundary. The momentum-conserving specular scattering ($p = 1$) does not add to thermal resistance. Only diffuse phonon scattering from rough interfaces ($p \longrightarrow 0$), which changes the phonon momentum, limits the phonon MFP. One can find p from the surface roughness or use it as a fitting parameter to experimental data. The commonly used expression for the phonon specularity is given by[29,33,34]

$$p(\lambda) = \exp\left(-\frac{16\pi^2\eta^2}{\lambda^2}\right) \tag{5}$$

where η is the root mean square deviation of the height of the surface from the reference plane and λ is the wavelength of the incident phonon.

In the case when phonon-boundary scattering is dominant, thermal conductivity scales with the nanostructure or grain size D as $K_{\mathrm{p}} \sim C_{\mathrm{p}}\upsilon\Lambda \sim C_{\mathrm{p}}\upsilon^2\tau_{\mathrm{B}} \sim C_{\mathrm{p}}\upsilon D$. In the very small structures with $D \ll \Lambda$, the thermal conductivity dependence on the physical size of the structure becomes more complicated due to the strong quantization of the phonon energy spectra.[6,30,32] The specific heat C_{p} depends on the phonon DOS, which leads to different $C_{\mathrm{p}}(T)$ dependences in 3-D, 2-D, and 1-D systems, and reflected in $K(T)$ dependence at low T.[26,29] In bulk at low T, $K(T) \sim T^3$, while it is $K(T) \sim T^2$ in 2-D systems.

Thermal conductivity K defines how well a given material conducts heat. Another characteristic—thermal diffusivity, α—defines how fast the material conducts heat. Thermal diffusivity is given by the expression

$$\alpha = \frac{K}{C_{\mathrm{p}}\rho_{\mathrm{m}}} \tag{6}$$

where ρ_{m} is the mass density. Many experimental techniques measure thermal diffusivity rather than thermal conductivity.

EXPERIMENTAL DATA FOR THERMAL CONDUCTIVITY OF GRAPHENE

We start by providing a brief summary of the experimental data available for the thermal conductivity of graphene. The first measurements of heat conduction in graphene[35–40] were carried out at UC Riverside in 2007 (see Fig. 1). The investigation of phonon transport was made possible by the development of the optothermal Raman measurement

Graphene–Guests

Downloaded by [University of California, Riverside Libraries] at 15:37 29 October 2014

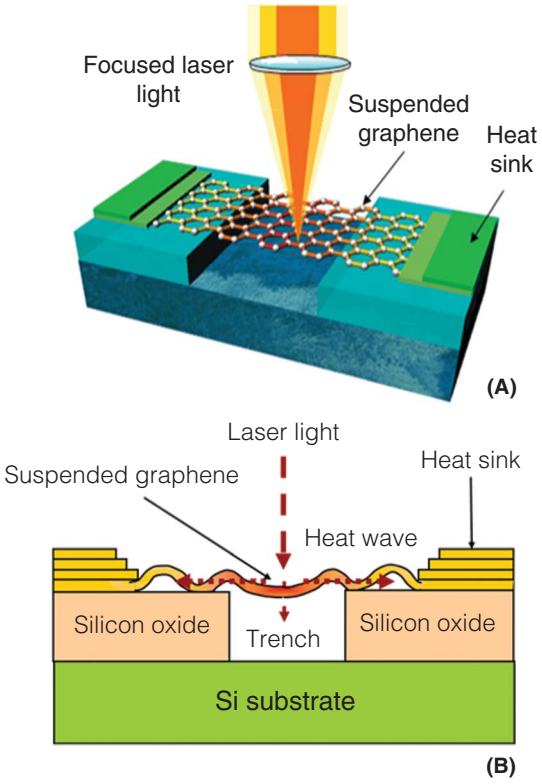

Fig. 1 (A) Schematic of the experimental setup with the excitation laser light focused on graphene suspended across a trench in Si wafer. Laser power absorbed in graphene induces a local hot spot and generates a heat wave propagating toward the heat sinks. (B) Illustration of the micro- and nanoscale corrugation formed in the suspended flake, which further reduce the thermal coupling to the substrate. The depicted experimental technique allows one for the steady-state non-contact direct measurement of the thermal conductivity.
Source: From Ghosh, Nika, et al.[37] © 2009 Institute of Physics and Deutsche Physikalische Gesellschaft.

technique. Balandin and coworkers[35,36] took advantage of the fact that graphene has distinctive signatures in Raman spectra with a clear *G* peak and 2-D band.[41–45] Moreover, they also found that the *G* peak of graphene's Raman spectra exhibits strong temperature dependence.[41] The latter means that the shift in the position of *G* peak in response to laser heating can be used for measuring the local temperature rise. The correlation between the temperature rise and the amount of power dissipated in graphene, for the sample with given geometry and proper heat sinks, can give the value of the thermal conductivity *K* (see the schematic of the experiment in Fig. 1A). Even a small amount of power dissipated in graphene can be sufficient for inducing a measurable shift in the *G* peak position due to the extremely small thickness of the material—one atomic layer. The suspended portion of graphene served several essential functions for 1) accurately determining the amount of power absorbed by graphene through the calibration procedure; 2) forming 2-D in-plane heat front propagating toward the heat sinks; and 3) reducing the thermal coupling to the substrate through the increased micro- and nanoscale corrugations (see Fig. 1A).

The long graphene flakes for these measurements were produced using the standard technique of mechanical exfoliation of bulk Kish and highly oriented pyrolytic graphite (HOPG).[46–48] The trenches were fabricated using reactive ion etching. The width of these trenches ranged from 1 to 5 μm with the nominal depth of 300 nm. The single-layer graphene (SLG) flakes were selected using the micro-Raman spectroscopy by checking the intensity ratio of *G* and 2-D peaks and by 2-D band deconvolution.[43–45] The combination of these two Raman techniques with the atomic force microscopy (AFM) and scanning electron microscopy (SEM) allowed authors[35,36] to verify the number of atomic planes and flake uniformity with a high degree of accuracy. It was found that the thermal conductivity varies in a wide range and can exceed that of the bulk graphite, which is ~2000 W/mK at room temperature (RT). It was also determined that the electronic contribution to heat conduction in the ungated graphene near RT is much smaller than that of phonons, i.e., $K_e \ll K_p$. The phonon MFP in graphene was estimated to be on the order of 800 nm near RT (Fig. 2).[36]

Several independent studies, which followed, also utilized the Raman optothermal technique but modified it via the addition of a power meter under the suspended portion of graphene. It was found that the thermal conductivity of suspended high-quality chemical vapour-deposited (CVD) graphene exceeded ~2500 W/mK at 350 K, and it was as high as $K \approx 1400$ W/mK at 500 K.[49] The reported value was also larger than the thermal conductivity of bulk graphite at RT. Another Raman optothermal study with the suspended graphene found the thermal conductivity in the range of ~1500 to ~5000 W/mK.[50] Another group that repeated the Raman-based measurements found $K \approx 630$ W/mK for a suspended graphene membrane.[51] The differences in the actual temperature of graphene under laser heating, and strain distribution in the suspended graphene of various sizes and geometries can explain the data variation.

Another experimental study reported the thermal conductivity of graphene to be ~1800 W/mK at 325 K and ~710 W/mK at 500 K.[52] These values are lower than that of bulk graphite. However, instead of measuring light absorption in graphene under conditions of their experiment, Lee et al.[52] assumed that the optical absorption coefficient should be 2.3%. It is known that due to many-body effects, the absorption in graphene is the function of wavelength λ, when $\lambda > 1$ eV.[53–55] The absorption of 2.3% is observed only in the near-infrared at ~1 eV. The absorption steadily increases with decreasing λ (increasing energy). The 514.5 and 488 nm Raman laser lines

Graphene–Guests

Downloaded by [University of California, Riverside Libraries] at 15:37 29 October 2014

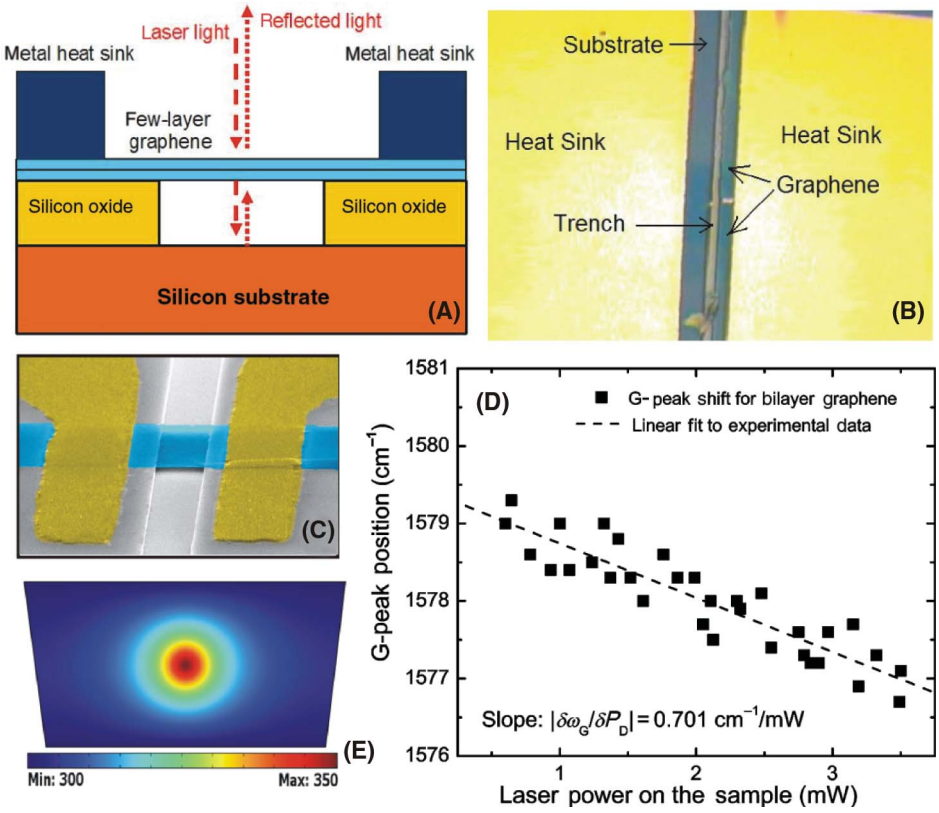

Fig. 2 Illustration of optothermal micro-Raman measurement technique developed for investigation of phonon transport in graphene. (A) Schematic of the thermal conductivity measurement showing suspended FLG flakes and excitation laser light. (B) Optical microscopy images of FLG attached to metal heat sinks. (C) Colored scanning electron microscopy image of the suspended graphene flake to clarify typical structure geometry. (D) Experimental data for Raman *G*-peak position change, $\delta\omega_G$, as a function of laser power change, δP_D, which determines the local temperature rise in response to the dissipated power. (E) Finite-element simulation of temperature distribution in the flake with the given geometry used to extract the thermal conductivity.

Source: From Ghosh, Bao, et al.[38] © 2010 Nature Publishing Group.

correspond to 2.41 and 2.54 eV, respectively. At 2.41 eV, the absorption is about $1.5 \times 2.3\% \approx 3.45\%$.[54] The value of 3.45% is in agreement with the one reported in another independent study.[56] Replacing the assumed 2.3% with 3.45% in the study by Lee et al.[52] gives ~2700 W/mK at 325 K and 1065 W/mK near 500 K. These values are higher than those for the bulk graphite and consistent with the data reported by other groups,[49,56] where the measurements were conducted by the same Raman optothermal technique but with measured light absorption.

The data for suspended or partially suspended graphene are closer to the intrinsic thermal conductivity, because suspension reduces thermal coupling to the substrate and scattering on the substrate defects and impurities. The thermal conductivity of fully supported graphene is smaller. The measurements for exfoliated graphene on SiO_2/Si revealed in-plane $K \approx 600$ W/mK near RT.[57] Solving the Boltzmann transport equation (BTE) and comparing with their experiments, the authors determined that the thermal conductivity of free graphene should be ~3000 W/mK near RT.

Despite the noted data scatter in the reported experimental values of the thermal conductivity of graphene, one can conclude that it is very large compared to that for bulk silicon ($K = 145$ W/mK at RT) or bulk copper ($K = 400$ W/mK at RT)—important materials for electronic applications. The differences in K of graphene can be attributed to variations in the graphene sample lateral sizes (length and width), thickness non-uniformity due to the mixing between single-layer and few-layer graphene (FLG), material quality (e.g., defect concentration and surface contaminations), grain size and orientation, as well as strain distributions. Often the reported thermal conductivity values of graphene corresponded to different sample temperatures T, despite the fact that measurements were conducted at ambient temperature. The strong heating of the samples was required due to the limited spectral resolution of the Raman spectrometers used for temperature measurements. Naturally, the thermal conductivity values determined at ambient but for the samples heated to $T \sim 350$ K and $T \sim 600$ K over a substantial portion of their area would be different and cannot be directly compared. One should also note that the data scatter for thermal conductivity of carbon nanotubes (CNTs) is much larger than that for graphene. For a more detailed analysis of the experimental uncertainties, readers are referred to comprehensive reviews.[16,58]

PHONON TRANSPORT IN SUSPENDED FLG

The phonon thermal conductivity undergoes an interesting evolution when the system dimensionality changes from 2-D to 3-D. This evolution can be studied with the help of suspended FLG with increasing thickness H—the number of atomic planes n. It was reported by Ghosh et al.[38] that the thermal conductivity of suspended uncapped FLG decreases with increasing n, approaching the bulk graphite limit (see Fig. 3). This trend was explained by considering the

Graphene–Guests

Downloaded by [University of California, Riverside Libraries] at 15:37 29 October 2014

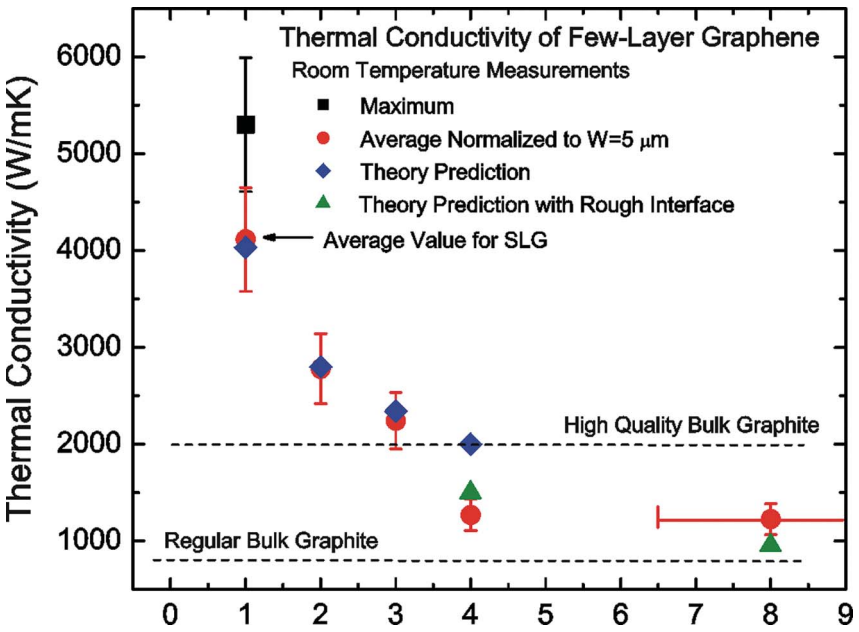

Fig. 3 Measured thermal conductivity as a function of the number of atomic planes in FLG. The dashed straight lines indicate the range of bulk graphite thermal conductivities. The blue diamonds were obtained from the first-principles theory of thermal conduction in FLG based on the actual phonon dispersion and accounting for all allowed three-phonon Umklapp scattering channels. The green triangles are Callaway–Klemens model calculations, which include extrinsic effects characteristic for thicker films.
Source: From Ghosh, Bao, et al.[38]

intrinsic quasi-2-D crystal properties described by the phonon Umklapp scattering.[38] As n in FLG increases, the phonon dispersion changes and more phase-space states become available for phonon scattering, leading to thermal conductivity decrease. The phonon scattering from the top and bottom boundaries in suspended FLG is limited if constant n is maintained over the layer length. The small thickness of FLG ($n < 4$) also means that phonons do not have a transverse cross-plane component in their group velocity, leading to even weaker boundary scattering term for the phonons. In thicker FLG films, the boundary scattering can increase due to the non-zero cross-plane phonon velocity component. It is also harder to maintain constant thickness throughout the whole area of the FLG flake. These factors can lead to a thermal conductivity below the graphite limit. The graphite value is recovered for thicker films.

The experimentally observed evolution of the thermal conductivity in FLG with n varying from 1 to $\sim$4[38] is in agreement with the theory for crystal lattices described by the Fermi–Pasta–Ulam Hamiltonians.[59] The molecular-dynamics (MD) calculations for graphene nanoribbons (GNRs) with the number of planes n from 1 to 8[60] also gave the thickness dependence of the thermal conductivity in agreement with the UC Riverside experiments.[38] The strong reduction of the thermal conductivity as n changes from 1 to 2 is in line with the earlier theoretical predictions.[61] In another reported study, the BTE was solved under the assumptions that in-plane interactions are described by the Tersoff potential, while the Lennard-Jones potential models the interactions between atoms belonging to different layers.[62,63] The obtained results suggested a strong thermal conductivity decrease as n changed from 1 to 2 and slower decrease for $n > 2$.

The thermal conductivity dependence on the FLG is entirely different for the encased FLG, where thermal transport is limited by the acoustic phonon scattering from the top and bottom boundaries and disorder. The latter is common when FLG is embedded between two layers of dielectrics. An experimental study[64] found $K \approx 160$ W/mK for encased SLG at $T = 310$ K. It increases to $\sim$1000 W/mK for graphite films with the thickness of 8 nm. It was also found that the suppression of thermal conductivity in encased graphene, as compared to bulk graphite, was stronger at low temperatures where K was proportional to T^{β} with $1.5 < \beta < 2$.[64] Thermal conduction in encased FLG was limited by rough boundary scattering and disorder penetration through graphene.

PHONON SPECTRA IN GRAPHENE, FLG, AND GNRS

Intriguing thermal and electrical properties of graphene, FLG,[16,35–38,46–48] and GNRs[65–67] stimulate investigations of phonon energy spectra in these materials and structures.[68–82] The phonon energy spectrum is important for determining the sound velocity, phonon DOS, phonon–phonon or electron–phonon scattering rates, lattice heat capacity, as well as the phonon thermal conductivity. The optical phonon properties manifest themselves in Raman measurements. The number of graphene layers, their quality, and stacking order can be clearly distinguished using the Raman spectroscopy.[38,41,42,83,84] For these reasons, significant efforts have been made to accurately determine the phonon energy dispersion in graphite,[68–71]

Graphene–Guests

Downloaded by [University of California, Riverside Libraries] at 15:37 29 October 2014

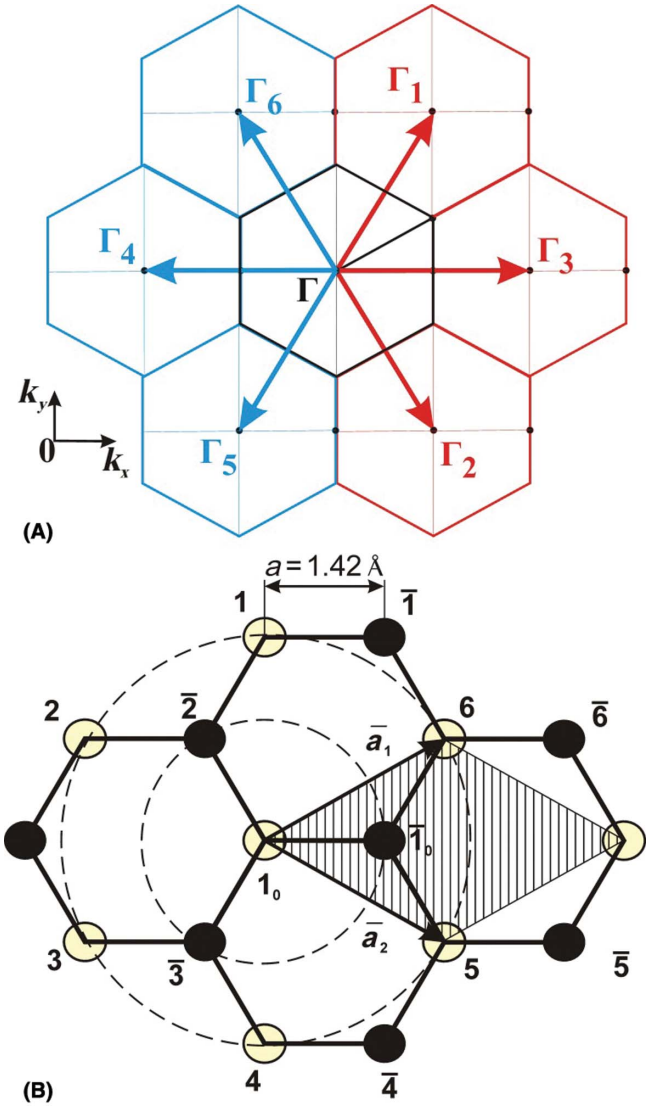

Fig. 4 (A) Reciprocal lattice of graphene. (B) Graphene crystal lattice. The rhombic unit cell is shown as a shaded region.
Source: From Nika, Pokatilov, et al.[82] © 2009 American Physical Society.

graphene,[38,62,72–77,82] and GNRs,[78–81,85] and to reveal specific features of their phonon modes.

The phonon dispersion in graphite along $\Gamma - M - K - \Gamma$ directions (see Fig. 4A, where the graphene Brillouin zone is shown) measured by X-ray inelastic scattering was reported by Maultzsch et al.[68] and Mohr et al.[69] A number of research groups calculated the phonon energy dispersion in graphite, graphene, and GNRs using various theoretical approaches, including continuum model,[80,81] Perdew–Burke–Ernzerhof generalized gradient approximation (GGA),[68,70,71] first-order local density approximation (LDA),[70,72,76] fourth- and fifth-nearest-neighbor force constant (4NNFC and 5NNFC) approaches,[69,71,77] Born–von Karman or valence force field (VFF) models of the lattice dynamics,[38,73,74,82] utilizing the Tersoff and Brenner potentials[75] or Tersoff and Lennard-Jones potentials.[62,63] These models (with the exception of GGA and LDA models) are based on different sets of the fitting parameters, which are usually determined from comparison with the experimental phonon dispersion, thermal expansion, or heat capacity.[68,69,86]

The number of parameters in the theoretical models depends on the model specifics and the number of considered atomic neighbors. The number of parameters varies from 5[71] to 23.[77] For example, VFF model developed for graphene by Nika et al.[82] used only six parameters. In this model, all interatomic forces are resolved into bond-stretching and bond-bending forces.[82,87–89] This model takes into account stretching and bending interactions with two in-plane and two out-of-plane atomic neighbors as well as doubled stretching–stretching interactions with the nearest in-plane neighbors.[82] The honeycomb crystal

Graphene–Guests

Downloaded by [University of California, Riverside Libraries] at 15:37 29 October 2014

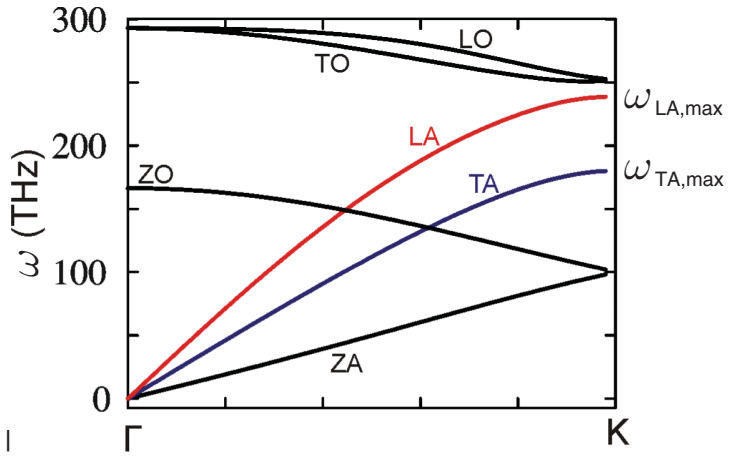

Fig. 5 Phonon frequencies ω_s in graphene calculated using the VFF model.
Source: From Ghosh, Nika, et al.[37] © 2009 Institute of Physics and Deutsche Physikalische Gesellschaft.

lattice of graphene utilized in this model is presented in Fig. 4B. The rhombic unit cell of graphene, shown as a dashed region, contains two atoms and is defined by two basis vectors $\vec{a}_1 = a(3, \sqrt{3})/2$ and $\vec{a}_2 = a(3, -\sqrt{3})/2$, where $a = 0.142$ nm is the distance between two nearest carbon atoms. The six phonon polarization branches $s = 1, \ldots, 6$ in SLG are shown in Fig. 5. These branches are 1) out-of-plane acoustic (ZA) and out-of-plane optical (ZO) phonons with the displacement vector along the z-axis; 2) transverse acoustic (TA) and transverse optical (TO) phonons, which correspond to the transverse vibrations within the graphene plane; and 3) longitudinal acoustic (LA) and longitudinal optical (LO) phonons, which correspond to the longitudinal vibrations within the graphene plane.

Although various theoretical models are in qualitative agreement with each other, they predict substantially different phonon frequencies at the Γ, M, or K points of the Brillouin zone. Moreover, some of the models give the same frequencies for the LO–LA phonons[71,72,75] and ZO–TA phonons[69,70,73,82] at the M point while the rest of the models predict different frequencies for these phonons at the M point.[68,74,76] The comparison between phonon frequencies at the high-symmetry points of the Brillouin zone is presented in Tables 1 and 2. The discrepancy in the calculated phonon dispersion can easily translate into differences in the predicted thermal conductivity values. Specifically, the relative contribution of the LA, TA, and ZA phonons to heat transport may vary in a wide range depending on the specifics of the phonon dispersion used.

The unit cell of the n-layer graphene contains $2{\cdot}n$ atoms; therefore, $6{\cdot}n$ quantized phonon branches appear in n-layer graphene. In Fig. 6A and B, we show the phonon dispersions in bilayer graphene. Weak van der Waals interaction between monolayers leads to the coupling of long-wavelength phonons only and quantization of the low-energy part of the spectrum with $q < 0.1q_{\max}$ for LA, TA, LO, TO, and ZO phonons and with $q < 0.4q_{\max}$ for ZA phonons (see Fig. 6B). The modification of the phonon energy spectrum in n-layer graphene as compared with that in SLG results in a substantial change of the

Table 1 Energies of ZO and LO phonons at Γ point in graphite and graphene.

Samples	Γ_{ZO} (cm^{-1})	Γ_{LO} (cm^{-1})	Comments
Graphite	—	1583[a]	Experiment: X-ray scattering
Graphite	—	1581[b]	Experiment: X-ray scattering
Graphite	899[c]	1593[c]	Theory: LDA
Graphite	~820[a], 879[c], 881[c]	1559[c], 1561[c], 1581–1582[a]	Theory: GGA
Graphite	868[b]	1577[b]	Theory: 5NNFC
Graphite	~920[d]	~1610[d]	Theory: six-parameter force constant model
Graphene	879[c], 881[c], 884[e]	1554[c], 1559[c], 1569[e]	Theory: GGA
Graphene	890[g], 896[g], ~900[f]	1586[f], 1595[g], 1597[g]	Theory: LDA
Graphene	893	1581	Theory: Born-von Karman
Graphene	889[h], 883.5[i]	1588[h], 1555[i]	Theory: VFF model
Graphene	~1300	~1685	Theory: optimized Tersoff
	~1165	~1765	Theory: optimized Brenner

Note: [a]Maultzsch, Reich, et al.[68]; [b]Mohr, Maultzsch, et al.[69]; [c]Mounet and Marzari[70]; [d]Aizawa, Sounda, et al.[86]; [e]Wirtz and Rubio[71]; [f] Yan, Ruan, et al.[72]; [g]Dubay and Kresse[76]; [h]Perebeinos and Tersoff[74]; [i]Nika, Pokatilov, et al.[82]; [j]Falkovsky[73]; [k]Lindsay and Broido.[75]

Downloaded by [University of California, Riverside Libraries] at 15:37 29 October 2014

Table 2 Phonon energies at K and M points in graphite and graphene.

Samples	$K_{ZA}(cm^{-1})$	$K_{TA}(cm^{-1})$	$K_{LA}(cm^{-1})$	Comments
Graphite	—	—	1194[a]	Experiment: X-ray scattering; $\omega_{LO}(M) > \omega_{LA}(M)$;
Graphite	542[b]	1007[b]	1218[b]	Experiment: X-ray scattering; $\omega_{LO}(M) > \omega_{LA}(M)$; $\omega_{ZO}(M) \approx \omega_{TA}(M)$
Graphite	—	—	—	Experiment: high-resolution electron-energy-loss spectroscopy; $\omega_{LO}(M) > \omega_{LA}(M)$; $\omega_{ZO}(M) < \omega_{TA}(M)$
Graphite	540[c]	1009[c]	1239[c]	Theory: LDA; $\omega_{LO}(M) > \omega_{LA}(M)$; $\omega_{ZO}(M) \approx \omega_{TA}(M)$
Graphite	534[c], 540[c]	~960[a], 998[c], 999[c]	1220[a], 1216[c], 1218[c]	Theory: GGA; $\omega_{LO}(M) > \omega_{LA}(M)$[ac]; $\omega_{ZO}(M) \approx \omega_{TA}(M)$[c]
Graphite	542[b]	1007[b]	1218[b]	Theory: 5NNFC; $\omega_{LO}(M) > \omega_{LA}(M)$; $\omega_{ZO}(M) \approx \omega_{TA}(M)$
Graphene	535[c], 539[d]	997[c], 1004[d]	1213[c], 1221[d]	Theory: GGA; $\omega_{LO}(M) > \omega_{LA}(M)$[c]; $\omega_{LO}(M) \approx \omega_{LA}(M)$[d]; $\omega_{ZO}(M) \approx \omega_{TA}(M)$[c,d]
Graphene	~520[e,f]	~990[f] ~1000[e]	~1250[f], ~1220[e]	Theory: LDA; $\omega_{LO}(M) \approx \omega_{LA}(M)$[e]; $\omega_{ZO}(M) \approx\approx \omega_{ZA}(M) << \omega_{TA}(M)$[e]; $\omega_{LO}(M) > \omega_{LA}(M)$[f]; $\omega_{ZO}(M) > \omega_{ZA}(M)$[f];
Graphene	495	1028	1199	Theory: Born-von Karman model; $\omega_{LO}(M) > \omega_{LA}(M)$; $\omega_{ZO}(M) \approx \omega_{TA}(M)$
Graphene	544[g], 532[h]	1110[g], 957[h]	1177[g], 1267[h]	Theory: VFF model; $\omega_{LO}(M) > \omega_{LA}(M)$[g,h]; $\omega_{ZO}(M) < \omega_{TA}(M)$[g]; $\omega_{ZO}(M) \approx \omega_{TA}(M)$[h]
Graphene	~635	~1170	~1170	Theory: optimized Tersoff potential; $\omega_{LO}(M) \approx \omega_{LA}(M)$; $\omega_{ZO}(M) > \omega_{TA}(M)$
	~585	~1010	~1240	Theory: optimized Brenner potential; $\omega_{LO}(M) > \omega_{LA}(M)$; $\omega_{ZO}(M) > \omega_{TA}(M)$

Note: [a]Maultzsch, Reich, et al.[68]; [b]Mohr, Maultzsch, et al.[69]; [c]Mounet and Marzari[70]; [d]Wirtz and Rubio[71]; [e]Yan, Ruan, et al.[72]; [f]Dubay and Kresse[76]; [g]Perebeinos and Tersoff[74]; [h]Nika, Pokatilov, et al.[82]; [i]Aizawa, Sounda, et al.[86]; [j]Falkovsky[73]; [k]Lindsay and Broido.[75]

Graphene–Guests

Downloaded by [University of California, Riverside Libraries] at 15:37 29 October 2014

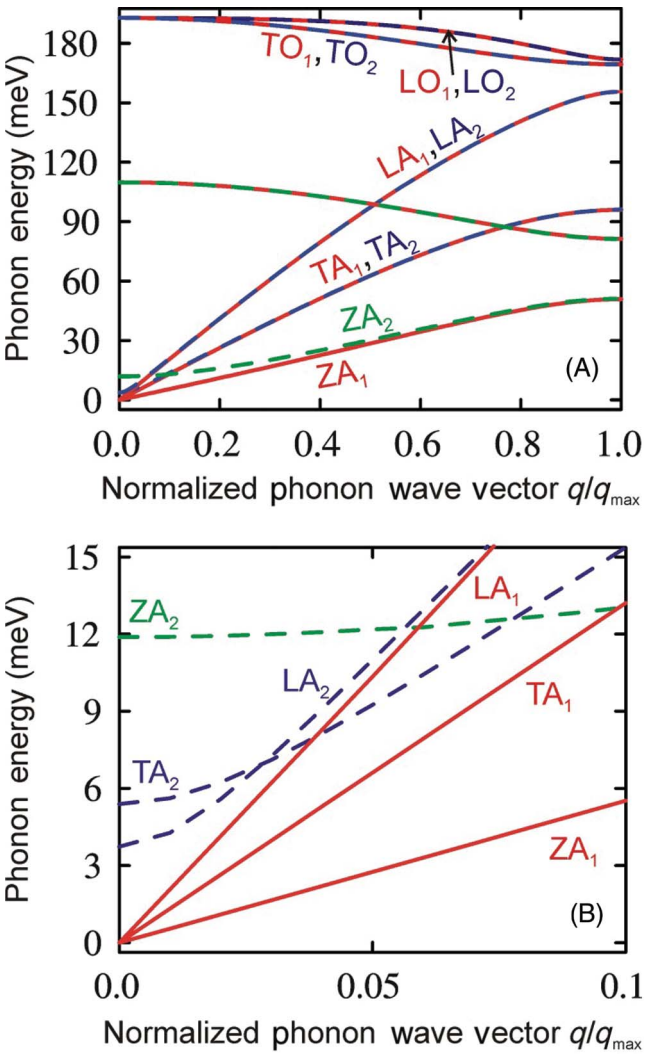

Fig. 6 Phonon energy spectra in bilayer graphene calculated using the VFF model shown for (A) Γ–M direction and (B) near the Brillouin zone center.
Source: From Ghosh, Bao, et al.[38] © 2010 Nature Publishing Group.

three-phonon scattering rates and a reduction of the intrinsic thermal conductivity in *n*-layer graphene.[38,62,63]

SPECIFICS OF THE ACOUSTIC PHONON TRANSPORT IN TWO-DIMENSIONAL CRYSTALS

We now address in more detail some specifics of the acoustic phonon transport in 2-D systems. Investigation of the heat conduction in graphene[35,36] and CNTs[90] raised the issue of ambiguity in the definition of the intrinsic thermal conductivity for 2-D and 1-D crystal lattices. It was theoretically shown that the intrinsic thermal conductivity limited by the crystal anharmonicity has a finite value in 3-D bulk crystals.[12,59] However, many theoretical models predict that the intrinsic thermal conductivity reveals a logarithmic divergence in strictly 2-D systems, $K \sim \ln(N)$, and a power-law divergence in 1-D systems, $K \sim N^{\alpha}$, with the number of atoms N ($0 < \alpha < 1$).[12,17,59,90–94] The logarithmic divergence can be removed by the introduction of *extrinsic* scattering mechanisms such as scattering from defects or coupling to the substrate.[59] Alternatively, one can define the *intrinsic* thermal conductivity of a 2-D crystal for a given size of the crystal.

Graphene is not an ideal 2-D crystal, considered so in most of the theoretical works, since graphene atoms vibrate in three directions. Nevertheless, the intrinsic graphene thermal conductivity strongly depends on the graphene sheet size due to weak scattering of the low-energy phonons by other phonons in the system. Therefore, the phonon-boundary scattering is an important mechanism for phonon relaxation in graphene. Different studies[95–97] also suggested that an accurate accounting of the higher-order anharmonic processes, i.e., above three-phonon Umklapp scattering, and inclusion of the normal phonon processes into consideration allow one to limit the low-energy phonon MFP. The normal phonon processes do not contribute directly to thermal resistance but affect the phonon mode distribution.[62,97,98] However, even these studies found that the graphene sample has to be very large (>10 μm) to obtain size-independent thermal conductivity.

The specific phonon transport in a quasi-2-D system such as graphene can be illustrated with an expression derived by Klemens specifically for graphene.[25,99] In the framework of the BTE approach and the RTA, the intrinsic Umklapp-limited thermal conductivity of graphene can be written as[25,99]

$$K = \frac{\rho_{\mathrm{m}}}{2\pi\gamma^2}\frac{\bar{v}^4}{f_{\mathrm{m}}T}\ln\left(\frac{f_{\mathrm{m}}}{f_{\mathrm{B}}}\right) \tag{7}$$

Here, f_{m} is the upper limit of the phonon frequencies defined by the phonon dispersion, $\bar{v}$ is the average phonon group velocity, $f_{\mathrm{B}} = (M\bar{v}^3 f_{\mathrm{m}}/4\pi\gamma^2 k_{\mathrm{B}}\mathrm{TL})^{1/2}$ is the size-dependent low-bound cutoff frequency for acoustic phonons, introduced by limiting the phonon MFP with the graphene layer size L.

In Nika et al.'s[100] work, Eq. 7 was improved by taking into account the actual maximum phonon frequencies and Grüneisen parameters γ_s ($s = TA, LA$) determined separately for LA and TA phonon branches. The Grüneisen parameters were computed by averaging the phonon mode-dependent $\gamma_s(\vec{q})$ for all relevant phonons (here $\vec{q}$ is the wave vector):

$$K = \frac{1}{4\pi k_{\mathrm{B}}T^2 h}\sum_{s=\mathrm{TA,LA}}\int_{q_{\min}}^{q_{\max}}\left\{\left[\hbar\omega_s(q)\frac{d\omega_s(q)}{dq}\right]^2\tau_{U,s}^{K}(q) \times \frac{\exp[\hbar\omega_s(q)/k_{\mathrm{B}}T]}{[\exp[\hbar\omega_s(q)/k_{\mathrm{B}}T]-1]^2}q\right\}dq \tag{8}$$

Downloaded by [University of California, Riverside Libraries] at 15:37 29 October 2014

Here, $\hbar\omega_s(q)$ is the phonon energy, $h = 0.335$ nm is the graphene layer thickness, and $\tau^K_{U,s}(q)$ is the three-phonon mode-dependent Umklapp relaxation time, which was derived using an expression from Klemens[25,26] but introducing separate lifetimes for LA and TA phonons:

$$\tau^K_{U,s} = \frac{1}{\gamma_s^2}\frac{M\bar{v}_s^2}{k_B T}\frac{\omega_{s,\max}}{\omega^2} \tag{9}$$

where $s = $ TA, LA, $\bar{v}_s$ is the average phonon velocity for a given branch, $\omega_{s,\max} = \omega(q_{\max})$ is the maximum cutoff frequency for a given branch, and M is the mass of a graphene unit cell. In Klemens[25,99] and Nika et al.,[100] the contribution of ZA phonons to thermal transport has been neglected because of their low group velocity and large Grüneisen parameter γ_{ZA}.[70,100] Eq. 9 can be used to calculate thermal conductivity with the actual dependence of the phonon frequency $\omega_s(q)$ and the phonon velocity $d\omega_s(q)/dq$ on the phonon wave number. To simplify the model, one can use the liner dispersion $\omega_s(q) = \bar{v}_s q$ and rewrite it as

$$K_U = \frac{\hbar^2}{4\pi k_B T^2 h}\sum_{s=\mathrm{TA,LA}} \times \int_{\omega_{\min}}^{\omega_{\max}} \left\{\omega^3 \tau^K_{U,s}(\omega)\frac{\exp[\hbar\omega/kT]}{[\exp[\hbar\omega/kT]-1]^2}\right\} d\omega \tag{10}$$

Substituting Eq. 9 into Eq. 10 and performing integration, one obtains

$$K_U = \frac{M}{4\pi T h}\sum_{s=\mathrm{TA,LA}} \frac{\omega_{s,\max}\bar{v}_s^2}{\gamma_s^2} F\left(\omega_{s,\min}, \omega_{s,\max}\right) \tag{11}$$

where

$$\begin{aligned} F\left(\omega_{s,\min}, \omega_{s,\max}\right) &= \int_{\hbar\omega_{s,\min}/k_B T}^{\hbar\omega_{s,\max}/k_B T} \xi \frac{\exp(\xi)}{[\exp(\xi)-1]^2} d\xi \\ &= \Big[\ln\{\exp(\xi)-1\}. \\ &\quad + \frac{\xi}{1-\exp(\xi)} - \xi\Big]\Big|_{\hbar\omega_{s,\min}/k_B T}^{\hbar\omega_{s,\max}/k_B T} \end{aligned} \tag{12}$$

In the above equation, $\xi = \hbar\omega/k_B T$, and the upper cutoff frequencies $\omega_{s,\max}$ are defined from the actual phonon dispersion in graphene (see Fig. 5): $\omega_{\mathrm{LA,max}} = 2\pi f_{\mathrm{LA,max}}(\Gamma K) = 241\ \mathrm{ps}^{-1}$, $\omega_{\mathrm{TA,max}} = 2\pi f_{\mathrm{TA,max}}(TK) = 180\ \mathrm{ps}^{-1}$.

The integrand in Eq. 12 can be further simplified near RT when $\hbar\omega_{s,\max} > k_B T$, and it can be expressed as

$$\begin{aligned} F\left(\omega_{s,\min}\right) \approx &-\ln\left\{\left|\exp\left(\hbar\omega_{s,\min}/k_B T\right) - 1\right|\right\} \\ &+ \frac{\hbar\omega_{s,\min}}{k_B T}\frac{\exp(\hbar\omega_{s,\min}/k_B T)}{\exp(\hbar\omega_{s,\min}/k_B T) - 1} \end{aligned} \tag{13}$$

There is a clear difference between the heat transport in basal planes of bulk graphite and in SLG.[25,99] In the former, the heat transport is approximately 2-D only up to some lower-bound cutoff frequency $\omega_{\min}$. Below $\omega_{\min}$ there appears to be strong coupling with the cross-plane phonon modes, and heat starts to propagate in all directions, which reduces the contributions of these low-energy modes to heat transport along basal planes to negligible values. In bulk graphite, there is a physically reasonable reference point for the onset of the cross-plane coupling, which is the ZO′ phonon branch near ~4 THz observed in the spectrum of bulk graphite.[25,101] The presence of the ZO′ branch and corresponding $\omega_{\min} = \omega_{\mathrm{ZO'}}(q = 0)$ allows one to avoid the logarithmic divergence in the Umklapp-limited thermal conductivity integral (see Eqs. 10–13) and calculate it without considering other scattering mechanisms.

The physics of heat conduction is principally different in graphene where the phonon transport is 2-D all the way to zero phonon frequency $\omega(q = 0) = 0$. There is no onset of the cross-plane heat transport at the long-wavelength limit in the system, which consists of only one atomic plane. This is no ZO′ branch in the phonon dispersion of graphene (see Fig. 5). Therefore, the lower-bound cutoff frequencies $\omega_{s,\min}$ for each s are determined from the condition that the phonon MFP cannot exceed the physical size L of the flake, i.e.,

$$\omega_{s,\min} = \frac{\bar{v}_s}{\gamma_s}\sqrt{\frac{M\bar{v}_s}{k_B T}\frac{\omega_{s,\max}}{L}} \tag{14}$$

We would like to emphasize here that using size-independent graphite $\omega_{\min}$ for SLG or FLG (as has been proposed by Kong et al.[102]) is without scientific merit and leads to an erroneous calculation of thermal conductivity, as described in detail by Nika et al.[103] Equations 12–14 constitute a simple analytical model for the calculation of the thermal conductivity of the graphene layer, which retains such important features of graphene phonon spectra as different $\bar{v}_s$ and γ_s for LA and TA branches. The model also reflects the 2-D nature of the heat transport in graphene all the way down to zero phonon frequency.

In Fig. 7, we present the dependence of thermal conductivity of graphene on the dimension of the flake L. The data are presented for the averaged values of the Grüneisen parameters $\gamma_{\mathrm{LA}} = 1.8$ and $\gamma_{\mathrm{TA}} = 0.75$ obtained from *ab initio* calculations, as well as for several other close sets of $\gamma_{\mathrm{LA,TA}}$ to illustrate the sensitivity of the result to the Grüneisen parameters. For small graphene flakes, the K dependence on L is rather strong. It weakens for flakes with $L \geq 10$ μm. The calculated values are in good agreement with available experimental data for suspended exfoliated[35,36] and CVD graphene.[49,50] The horizontal dashed line indicates the experimental thermal conductivity for bulk graphite, which is exceeded by graphene's thermal

Graphene–Guests

Downloaded by [University of California, Riverside Libraries] at 15:37 29 October 2014

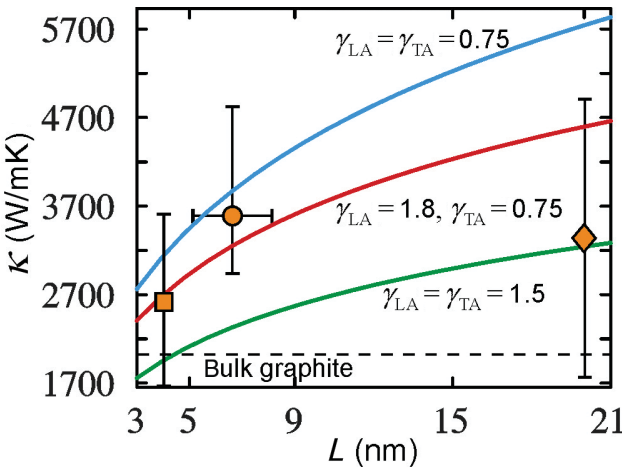

Fig. 7 Calculated RT thermal conductivity of graphene as a function of the lateral size for several values of the Grüneisen parameter. Experimental data points from Balandin et al.[35] and Ghosh et al.[36] (circle), Cai et al.[49] (square), and Jauregui et al.[50] (rhombus) are shown for comparison.
Source: From Nika & Balandin.[112] © 2012 IOP.

conductivity at smaller L. Thermal conductivity, presented in Fig. 7, is an *intrinsic* quantity limited by the three-phonon Umklapp scattering only. But it is determined for a specific graphene flake size since L defines the lower-bound (long-wavelength) cutoff frequency in Umklapp scattering through Eq. 14. In experiments, thermal conductivity is also limited by defect scattering. When the size of the flake becomes very large with many polycrystalline grains, the scattering on their boundaries will also lead to phonon relaxation. The latter can be included in our model through adjustment of L. The extrinsic phonon scattering mechanisms or high-order phonon–phonon scatterings prevent the indefinite growth of the thermal conductivity of graphene with L.

THE Q-SPACE DIAGRAM THEORY OF PHONON TRANSPORT IN GRAPHENE

The simple models described in the previous section are based on Klemens-like expressions for the relaxation time (see Eq. 9). Therefore, they do not take into account all peculiarities of the 2-D three-phonon Umklapp processes in SLG or FLG, which are important for the accurate description of thermal transport. There are two types of three-phonon Umklapp scattering processes.[26] The first type is the scattering when a phonon with the wave vector $\vec{q}(\omega)$ absorbs another phonon from the heat flux with the wave vector $\vec{q}'(\omega')$, i.e., the phonon leaves the state $\vec{q}$. For this type of scattering processes, the momentum and energy conservation laws are written as

$$\begin{aligned} &\vec{q}(\omega)+\vec{q}'(\omega')=\vec{b}_i+\vec{q}''(\omega''),\ i=1,2,3\\ &\omega+\omega'=\omega'' \end{aligned} \tag{15}$$

The processes of the second type are those when the phonons $\vec{q}(\omega)$ of the heat flux decay into two phonons with the wave vectors $\vec{q}'(\omega')$ and $\vec{q}''(\omega'')$, i.e., leave the state $\vec{q}(\omega)$, or, alternatively, two phonons $\vec{q}'(\omega')$ and $\vec{q}''(\omega'')$ merge together forming a phonon with the wave vector $\vec{q}(\omega)$, which corresponds to the phonon coming to the state $\vec{q}(\omega)$. The conservation laws for this type are given by

$$\begin{aligned} &\vec{q}(\omega)+\vec{b}_i=\vec{q}'(\omega')+\vec{q}''(\omega''),\quad i=4,5,6\\ &\omega=\omega'+\omega'' \end{aligned} \tag{16}$$

In Eqs. 15 and 16 $\vec{b}_i=\vec{\Gamma\Gamma}_i,\ i=1,2,...,6$ is one of the vectors of the reciprocal lattice (see Fig. 4A).

Calculations of the thermal conductivity in graphene taking into account all possible three-phonon Umklapp processes allowed by Eqs. 15 and 16 and actual phonon dispersions were carried out for the first time by Nika et al.[82] For each phonon mode (q_i,s) all pairs of the phonon modes $(\vec{q}',s')$ and $(\vec{q}'',s'')$ were found, such that the conditions of Eqs. 15 and 16 are met. As a result, in $(\vec{q}')$-space were constructed the *phase diagrams* for all allowed three-phonon transitions.[82] Using the long-wave approximation (LWA) for a matrix element of the three-phonon interaction, Nika et al.[82] obtained for the Umklapp scattering rates

$$\begin{aligned} \frac{1}{\tau_{\mathrm{U}}^{(\mathrm{I}),(\mathrm{II})}(s,\vec{q})}=\frac{\hbar\gamma_s^2(\vec{q})}{3\pi\rho\upsilon_s^2(\vec{q})}\sum_{s's'';\vec{b}_i}\iint\omega_s(\vec{q})\omega'_{s'}(\vec{q}')\omega''_{s''}(\vec{q}'')\times\\ \left\{N_0[\omega'_{s'}(\vec{q}')]\mp N_0[\omega''_{s''}(\vec{q}'')]+\frac{1}{2}\mp\frac{1}{2}\right\}\\ \times\delta\left[\omega_s(\vec{q})\pm\omega'_{s'}(\vec{q}')-\omega''_{s''}(\vec{q}'')\right]dq'_l dq'_\perp \end{aligned} \tag{17}$$

Here, q'_l and $q'_\perp$ are the components of the vector $\vec{q}'$ parallel or perpendicular to the lines defined by Eqs. 15 and 16, correspondingly, $\gamma_s(\vec{q})$ is the mode-dependent Grüneisen parameter, which is determined for each phonon wave vector and polarization branch, and ρ is the surface mass density. In Eq. 17, the upper signs correspond to the processes of the first type, while the lower signs correspond to those of the second type. The integrals for $q_l, q_\perp$ are taken along and perpendicular to the curve segments, correspondingly, where the conditions of Eqs. 15 and 16 are met. Integrating along q in Eq. 17, one can obtain the line integral

$$\begin{aligned} \frac{1}{\tau_{\mathrm{U}}^{(\mathrm{I}),(\mathrm{II})}(s,\vec{q})}=\frac{\hbar\gamma_s^2(\vec{q})\omega_s(\vec{q})}{3\pi\rho\upsilon_s^2(\vec{q})}\sum_{s's'';\vec{b}}\int_l\frac{\pm(\omega''_{s''}-\omega_s)\omega''_{s''}}{\upsilon_{\perp,s'}(\omega'_{s'})}\\ \times\left(N'_0\mp N''_0+\frac{1}{2}\mp\frac{1}{2}\right)dq'_l \end{aligned} \tag{18}$$

Downloaded by [University of California, Riverside Libraries] at 15:37 29 October 2014

The phonon scattering on the rough edges of graphene can be evaluated using Eq. 4. The total phonon relaxation rate is given by

$$\frac{1}{\tau_{\text{tot}}(s,q)} = \frac{1}{\tau_{\text{U}}(s,q)} + \frac{1}{\tau_{\text{B}}(s,q)} \tag{19}$$

The sensitivity of the RT thermal conductivity, calculated using Eqs. 17–19, to the value of the specular parameter of phonon-boundary scattering is illustrated in Fig. 8. The data are presented for different sizes (widths) of the graphene flakes. The experimental data points for suspended exfoliated[35–36] and CVD[49,50] graphene are also shown for comparison. Strong dependence of graphene thermal conductivity on tensile strain, flake size, van der Waals bond strength, as well as concentration of lattice defects, vacancies, and wrinkles was theoretically predicted.[104–111] Table 3 provides representative experimental and theoretical data for the suspended and supported graphene.

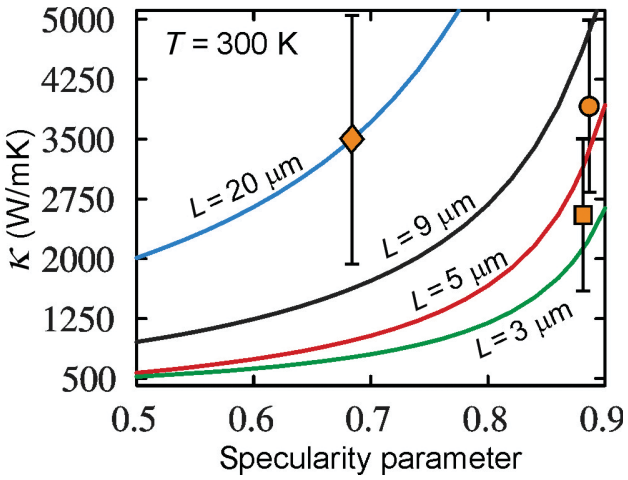

Fig. 8 Calculated RT thermal conductivity of suspended graphene as a function of the specularity parameter p for the phonon scattering from the flake edges. Note a strong dependence on the size of the graphene flakes. Experimental data points from Balandin et al.[35] and Ghosh et al.[36] (circle), Cai et al.[49] (square), and Jauregui et al.[50] (rhombus) are shown for comparison.
Source: From Nika & Balandin.[112]

THERMAL CONDUCTIVITY OF GNRs

Measurements of thermal properties of graphene stimulated a surge of interest in theoretical and experimental studies of

Table 3 Thermal conductivity of graphene and few-layer graphene.

Samples	K (W/mK)	Methods	Comments	Refs.
Graphene	~2000–5000	Raman optothermal	Suspended; exfoliated	[35, 36]
FLG	1300–2800	Raman optothermal	Suspended; exfoliated; $n = 2$–4	[38]
Graphene	~2500	Raman optothermal	Suspended; CVD	[49]
Graphene	~1500–5000	Raman optothermal	Suspended; CVD	[50]
Graphene	600	Raman optothermal	Suspended; exfoliated; $T \sim 660$ K	[51]
Graphene	600	Electrical	Supported; exfoliated;	[57]
Graphene	~1875 at T = 420 K	Micro-Raman mapping	Suspended CVD graphene membranes with and without wrinkles; wrinkles decreases the thermal conductivity by ~ 27%	[107]
Graphene	~2430	Theory: BTE, third-order IFCs	K(graphene) $\geq K$(carbon nanotube)	[98]
Graphene	1000–8000	Theory: BTE+RTA $\gamma_{\text{LA}}, \gamma_{\text{TA}}$	Strong size dependence	[100]
Graphene	2000–8000	Theory: BTE+RTA, γ_s (q)	Strong edge, width and Grüneisen parameter dependence	[82]
Graphene	~4000	Theory: ballistic	Strong width dependence	[66]
Graphene	~2900	Theory: MD simulation	Strong dependence on the vacancy concentration	[104]
Graphene	1500–3500	Theory: BTE, third-order IFCs	Strong size dependence	[108]
Graphene	~5000	Theory: BTE + RTA	Strong size and defect concentration dependence	[109]
Graphene	~1780 (suspended), ~ 480 (supported)	Theory: equilibrium molecular dynamics	Supported on copper; strong reduction of the thermal conductivity in supported graphene	[110]
FLG	1000–4000	Theory: BTE + RTA, γ_s (q)	$n = 8 - 1$, strong size dependence	[38]
FLG	1000–3500	Theory: BTE, third-order IFCs	$n = 5 - 1$, strong size dependence	[62]
FLG	2000–3300	Theory: BTE, third-order IFCs	$n = 4 - 1$	[63]
FLG	580–880	Theory: MD simulation	$n = 5 - 1$, strong dependence on the van der Waals bond strength	[111]

Graphene–Guests

Downloaded by [University of California, Riverside Libraries] at 15:37 29 October 2014

Table 4 Thermal conductivity of graphene nanoribbons.

Sample	*K*(W/mK)	Method	Comments	Refs.
FLG nanoribbon	1100	Electrical self-heating	Supported; exfoliated; $n < 5$	[109]
FLG nanoribbon	80–150	Electrical self-heating	Supported	[110]
GNR	1000–7000	Theory: molecular dynamics, Tersoff	Strong ribbon width and edge dependence	[59]
GNR	~5500	Theory: BTE + RTA	GNR with width of 5 μm; strong dependence on the edge roughness	[81]
GNR	400–600	Theory: equilibrium molecular dynamics	GNR with width of 4 nm; strong dependence on the GNR edge and thickness	[125]

heat conduction in GNRs.[65–67,85,113–121] It is important to understand how lateral sizes affect the phonon transport properties from both fundamental science and practical applications point of view. In the last few years, a number of theoretical works investigated phonon transport and heat conduction in GNRs with various lengths, widths, edge roughness, and defect concentrations. The authors used MD simulations,[65–67,113–116] non-equilibrium Green's function method,[117–119] and BTE approaches.[85,120]

Keblinsky and coworkers[65] found from the MD study that the thermal conductivity of graphene is $K \approx$ 8000–10,000 W/mK at RT for the square graphene sheet. The K value was size independent for $L > 5$ nm.[65] For the ribbons with fixed $L = 10$ nm and width W varying from 1 to 10 nm, K increased from ~1000 to 7000 W/mK. The thermal conductivity in GNR with rough edges can be suppressed by orders of magnitude as compared to that in GNR with perfect edges.[65,67] The isotopic superlattice modulation of GNR or defects of crystal lattices also significantly decreases the thermal conductivity.[118,119] The uniaxial stretching applied in the longitudinal direction enhances the low-temperature thermal conductance for the 5 nm armchair or zigzag GNR up to 36% due to the stretching-induced convergence of phonon spectra to the low-frequency region.[117] Aksamija and Knezevic[85] calculated the dependence of the thermal conductivity of GNR with the width 5 nm and RMS edge roughness $\Delta = 1$ nm on temperature. The thermal conductivity was calculated taking into account the three-phonon Umklapp, mass-defect, and rough edge scatterings.[85] The authors obtained RT thermal conductivity at $K \sim$ 5500 W/mK for the GNR. The study of non-linear thermal transport in rectangular and triangular GNRs under large temperature biases was reported by Hu et al.[121] The authors found that in short (~6 nm) rectangular GNRs, negative differential thermal conductance exists in a certain range of the applied temperature difference. As the length of the rectangular GNR increases, the effect weakens. A computational study reported by Xie et al.[122] predicted that the combined effects of the edge roughness and local defects play a dominant role in determining the thermal transport properties of zigzag GNRs. The experimental data on thermal transport in GNRs are very limited. Murali et al.[123] used electrical self-heating methods and extracted the thermal conductivity of sub-20 nm GNRs to be more than 1000 W/mK at 700–800 K. A similar experimental method but with a more accurate account of GNRs' thermal coupling to the substrate has been used by Liao et al.[124] Pop and coworkers[124] found substantially lower values of thermal conductivity of ~80–150 W/mK at RT. Wang et al.[125] employed equilibrium MD for investigation of the thermal conductivity in GNRs with zigzag and armchair edges and revealed the importance of edges to thermal conductivity in GNRs. The calculated and measured data for the thermal conductivity of GNRs are summarized in Table 4.

CONCLUSIONS

We reviewed the theoretical and experimental results pertinent to 2-D phonon transport in graphene. Phonons are the dominant heat carriers in the ungated graphene samples near RT. The unique nature of 2-D phonons, revealed in the very large phonon MFP and peculiarities of the DOS, translates to unusual heat conduction properties of graphene and related materials. Recent computational studies suggest that the thermal conductivity of graphene depends strongly on the concentration of defects, strain distribution, wrinkles, sample size and geometry. The revealed dependence can account for portion of the data scatter in reported experimental studies. Investigation of the physics of 2-D phonons in graphene can shed light on the thermal energy transfer in low-dimensional systems. The results presented in this entry are important for the proposed electronic and optoelectronic applications of graphene, and can lead to new methods of heat removal and thermal management.

ACKNOWLEDGMENTS

This work was supported, in part, by the National Science Foundation (NSF) projects U.S. EECS-1128304, EECS-1124733, and EECS-1102074, the U.S. Office of Naval Research (ONR) through award N00014-10-1-0224, Semiconductor Research Corporation (SRC) and Defense Advanced Research Project Agency (DARPA) through

FCRP Center on Functional Engineered Nano Architectonics (FENA), and DARPA-DMEA under agreement H94003-10-2-1003. DLN acknowledges the financial support through Moldova State Project No. 11.817.05.10F and 12.819.05.18F.

REFERENCES

1. Balandin, A.A. Better computing through CPU cooling. IEEE Spectrum. **2009**, 29–33.
2. Pop, E. Energy dissipation and transport in nanoscale devices. Nano Res. **2010**, *3*, 147.
3. Balandin, A.; Wang, K.L. Effect of phonon confinement on the thermoelectric figure of merit of quantum wells. J. Appl. Phys. **1998**, *84*, 6149.
4. Borca-Tasciuc, T.; Achimov, D.; Liu, W.L.; Chen, G.; Ren, H.-W.; Lin, C.-H.; Pei, S.S. Thermal conductivity of InAs/AlSb superlattices. Microscale Thermophys. Eng. **2001**, *5*, 225.
5. Li, D.; Wu, Y.; Kim, P.; Shi, L.; Yang, P.; Majumdar, A. Thermal conductivity of individual silicon nanowires. Appl. Phys. Lett. **2003**, *83*, 2934.
6. Balandin, A.A.; Pokatilov, E.P.; Nika, D.L. Phonon engineering in hetero- and nanostructures. J. Nanoelect. Optoelect. **2007**, *2*, 140.
7. Pokatilov, E.P.; Nika, D.L.; Balandin, A.A. Acoustic-phonon propagation in rectangular semiconductor nanowires with elastically dissimilar barriers. Phys. Rev. B **2005**, *72*, 113311.
8. Pokatilov, E.P.; Nika, D.L.; Balandin, A.A. Acoustic phonon engineering in coated cylindrical nanowires. Superlatt. Microstruct. **2005**, *38*, 168.
9. Liu, W.; Asheghi, M. Thermal conductivity measurements of ultra-thin single crystal silicon layers. J. Heat Transfer **2006**, *128*, 75.
10. Nika, D.L.; Zincenco, N.D.; Pokatilov, E.P. Engineering of thermal fluxes in phonon mismatched heterostructures. J. Nanoelect. Optoelect. **2009**, *4*, 180.
11. Lepri, S.; Livi, R.; Politi, A. Thermal conduction in classical low-dimensional lattices. Phys. Rep. **2003**, *377*, 1.
12. Basile, G.; Bernardin, C.; Olla, S. Momentum conversion model with anomalous thermal conductivity in low dimensional system. Phys. Rev. Lett. **2006**, *96*, 204303.
13. Pokatilov, E.P.; Nika, D.L.; Balandin, A.A. Phonon spectrum and group velocities in AlN/GaN/AlN and related heterostructures. Superlatt. Microstruct. **2003**, *33*, 155.
14. Pernot, G.; Stoffel, M.; Savic, I.; Pezzoli, F.; Chen, P.; Savelli, G.; Jacquot, A.; Schumann, J.; Denker, U.; Mönch, I.; Deneke, Gh.; Schmidt, O.G.; Rampnoux, J.M.; Wang, S.; Plissonnier, M.; Rastelli, A.; Dilhaire, S.; Mingo, N. Precise control of thermal conductivity at the nanoscale through individual phonon-scattering barriers. Nat. Mater. **2010**, *9*, 491.
15. Nika, D.L.; Pokatilov, E.P.; Balandin, A.A.; Fomin, V.M.; Rastelli, A.; Schmidt, O.G. Reduction of lattice thermal conductivity in one-dimensional quantum-dot superlattices due to phonon filtering. Phys. Rev. B **2011**, *84*, 165415.
16. Balandin, A.A. Thermal properties of graphene and nanostructured carbon materials. Nat. Mater. **2011**, *10*, 569.
17. Chang, C.W.; Okawa, D.; Garcia, H.; Majumdar, A.; Zettl, A. Breakdown of Fourier's law in nanotube thermal conductors. Phys. Rev. Lett. **2008**, *101*, 075903.
18. Narayan, O.; Ramaswamy, S. Anomalous heat conduction in one dimensional momentum-conserving systems. Phys. Rev. Lett. **2002**, *89*, 200601.
19. Cahill, D.G.; Ford, W.K.; Goodson, K.E.; Mahan, G.D.; Majumdar, A.; Maris, H.J.; Merlin, R.; Phillpot S.R. Nanoscale thermal transport. J. Appl. Phys. **2003**, *93*, 793.
20. Bhandari, C.M.; Rowe, D.M. *Thermal Conduction in Semiconductors*; Wiley & Sons: New York, 1988.
21. Srivastava, G.P. *The Physics of Phonons*; Taylor & Francis: New York, 1990.
22. Mills, A.F. *Heat and Mass Transfer*; Richard D. Irwin: Chicago, IL, 1995, 62.
23. Ziman, J.M. *Principles of the Theory of Solids,* 2nd Ed.; Cambridge University Press: New York, 2001, 232.
24. Pierson, H.O. *Handbook of Carbon, Graphite, Diamonds and Fullerenes: Processing, Properties and Applications*; Noyes Publications: Park Ridge, New Jersey, 2010.
25. Klemens, P.G. Theory of the a-plane thermal conductivity of graphite. J. Wide Bandgap Mater. **2000**, *7*, 332.
26. Klemens, P.G. Thermal conductivity and lattice vibrational modes. Solid State Phys. **1958**, *7*, 1(edited by F. Seitz and D. Turnbull (Academic, New York)).
27. Callaway, J. Model for lattice thermal conductivity at low temperatures. Phys. Rev. **1959**, *113*, 1046.
28. Parrott, J.E.; Stuckes, A.D. *Thermal Conductivity of Solids*; Methuen: New York, 1975.
29. Ziman, J.M. *Electrons and Phonons: The Theory of Transport Phenomena in Solids*; Oxford University Press: New York, 2001.
30. Balandin, A.; Wang, K.L. Significant decrease of the lattice thermal conductivity due to phonon confinement in a free-standing semiconductor quantum well. Phys. Rev. B **1998**, *58*, 1544.
31. Zou, J.; Balandin, A. Phonon heat conduction in a semiconductor nanowires. J. Appl. Phys. **2001**, *89*, 2932.
32. Balandin, A.A. Nanophononics: Phonon engineering in nanostructures and nanodevices. J. Nanosci. Nanotechol. **2005**, *5*, 1015.
33. Aksamija, Z.; Knezevic, I. Anisotropy and boundary scattering in the lattice thermal conductivity of silicon nanomembranes. Phys. Rev. B **2010**, *82*, 045319.
34. Soffer, S.B. Statistical model for the size effect in electrical conduction. J. App. Phys. **1967**, *38*, 1710.
35. Balandin, A.A.; Ghosh, S.; Bao, W.; Calizo, I.; Teweldebrhan, D.; Miao, F.; Lau, C.N. Superior thermal conductivity of single layer graphene. Nano Lett. **2008**, *8*, 902.
36. Ghosh, S.; Calizo, I.; Teweldebrhan, D.; Pokatilov, E.P.; Nika, D.L.; Balandin, A.A.; Bao, W.; Miao, F.; Lau, C.N. Extremely high thermal conductivity in graphene: Prospects for thermal management application in nanoelectronic circuits. Appl. Phys. Lett. **2008**, *92*, 151911.
37. Ghosh, S.; Nika, D.L.; Pokatilov, E.P.; Balandin, A.A. Heat conduction in graphene: Experimental study and theoretical interpretation. New J. Phys. **2009**, *11*, 095012.
38. Ghosh, S.; Bao, W.; Nika, D.L.; Subrina, S.; Pokatilov, E.P.; Lau, C.N.; Balandin, A.A. Dimensional crossover of thermal transport in few-layer graphene. Nat. Mater. **2010**, *9*, 555.

Downloaded by [University of California, Riverside Libraries] at 15:37 29 October 2014

Graphene–Guests

Downloaded by [University of California, Riverside Libraries] at 15:37 29 October 2014

39. Balandin, A.A.; Ghosh, S.; Nika, D.L.; Pokatilov, E.P. Extraordinary thermal conductivity of graphene: Possible applications in thermal management. ECS Trans. **2010**, *28*, 63.
40. Balandin, A.A.; Ghosh, S.; Nika, D.L.; Pokatilov, E.P. Thermal conduction in suspended graphene layers. Fullerenes Nanotubes Carbon Nanostruct. **2010**, *18*, 1.
41. Calizo, I.; Balandin, A.A.; Bao, W.; Miao, F.; Lau, C.N. Temperature dependence of the Raman spectra of graphene and graphene multilayers. Nano Lett. **2007**, *7*, 2645.
42. Graf, D.; Molitor, F.; Ensslin, K.; Stampfer, C.; Jungen, A.; Hierold, C.; Wirtz, L. Spatially resolved Raman spectroscopy of single- and few-layer graphene. Nano Lett. **2007**, *7*, 238.
43. Ferrari, A.C., Meyer, J. C., Scardaci, V., Casiraghi, C., Lazzeri, M., Mauri, F., Piscanec, S., Jiang, D., Novoselov, K. S., Roth, S., Geim, A. K. Raman spectrum of graphene and graphene layers. Phys. Rev. Lett **2006**, *97*, 187401.
44. Calizo, I.; Bao, W.; Miao, F.; Lau, C.N.; Balandin, A.A. The effect of substrates on the Raman spectrum of graphene: Graphene-on-sapphire and graphene-on-glass. Appl. Phys. Lett **2007**, *91*, 201904.
45. Calizo, I.; Teweldebrhan, D.; Bao, W.; Miao, F.; Lau, C.N.; Balandin, A.A. Spectroscopic Raman nanometrology of graphene and graphene multilayers on arbitrary substrates. J. Phys. C **2008**, *109*, 012008.
46. Novoselov, K.S.; Geim, A.K.; Morozov, S.V.; Jiang, D.; Zhang, Y.; Dubonos, S.V.; Grigorieva, I.V.; Firsov, A.A. Electric field effect in atomically thin carbon films. Science **2004**, *306*, 666.
47. Novoselov, K.S.; Geim, A.K.; Morozov, S.V.; Jiang, D.; Katsnelson, M.I.; Grigorieva, I.V.; Dubonosov, S.V.; Firsov, A.A. Two-dimensional gas of massless Dirac fermions in graphene 2005. Nature **2005**, *438*, 197.
48. Zhang, Y.B.; Tan, Y.W.; Stormer, H.L.; Kim, P. Experimental observation of the quantum Hall effect and Berry's phase in graphene. Nature **2005**, *438*, 201.
49. Cai, W.; Moore, A.L.; Zhu, Y.; Li, X.; Chen, S.; Shi, L.; Ruoff, R.S. Thermal transport in suspended and supported monolayer graphene grown by chemical vapor deposition. Nano Lett. **2010**, *10*, 1645.
50. Jauregui, L.A.; Yue, Y.; Sidorov, A.N.; Hu, J.; Yu, Q.; Lopez, G.; Jalilian, R.; Benjamin, D.K.; Delk, D.A.; Wu, W.; Liu, Z.; Wang, X.; Jiang, Z.; Ruan, X.; Bao, J.; Pei, S.S.; Chen, Y.P. Thermal transport in graphene nanostructures: Experiments and simulations. ECS Trans. **2010**, *28*, 73.
51. Faugeras, C.; Faugeras, B.; Orlita, M.; Potemski, M.; Nair, R.R.; Geim, A.K. Thermal conductivity of graphene in Corbino membrane geometry. ACS Nano **2010**, *4*, 1889.
52. Lee, J.U.; Yoon, D.; Kim, H.; Lee, S.W.; Cheong, H. Thermal conductivity of suspended pristine graphene measured by Raman spectroscopy. Phys. Rev. B **2011**, *83*, 081419.
53. Mak, K.F.; Shan, J.; Heinz, T.F. Seeing many-body effects in single and few layer graphene: Observation of two-dimensional saddle point excitons. Phys. Rev. Lett. **2011**, *106*, 046401.
54. Kim, K.S.; Zhao, Y.; Jang, H.; Lee, S.Y.; Kim, J.M.; Kim, K.S.; Ahn, J.; Kim, P.; Choi, J.; Hong, B.H. Large-scale pattern growth of graphene films for stretchable transparent electrodes. Nature **2009**, *457*, 706.
55. Kravets, V.G.; Grigorenko, A.N.; Nair, R.R.; Blake, P.; Anissimova, S.; Novoselov, K.S.; Geim, A.K. Spectroscopic ellipsometry of graphene and an exciton-shifted van Hove peak in absorption. Phys. Rev. B **2010**, *81*, 155413.
56. Chen, S.; Moore, A.L.; Cai, W.; Suk, J.W.; An, J.; Mishra, C.; Amos, C.; Magnuson, C.W.; Kang, J.; Shi, L.; Ruoff, R.S. Raman measurement of thermal transport in suspended monolayer graphene of variable sizes in vacuum and gaseous environments. ACS Nano **2011**, *5*, 321.
57. Seol, J.H.; Jo, I.; Moore, A.L.; Lindsay, L.; Aitken, Z.H.; Pettes, M.T.; Li, X.; Yao, Z.; Huang, R.; Broido, D.; Mingo, N.; Ruoff, R.S.; Shi, L. Two-dimensional phonon transport in supported graphene. Science **2010**, *328*, 213.
58. Balandin, A.A.; Nika, D.L. Phononics in low-dimensional materials. Mater. Today **2012**, *15*, 266.
59. Saito, K.; Dhar, A. Heat conduction in a three dimensional anharmonic crystal. Phys. Rev. Lett. **2010**, *104*, 040601.
60. Zhong, W.R.; Zhang, M.P.; Ai, B.Q.; Zheng, D.Q. Chirality and thickness-dependent thermal conductivity of few-layer graphene: A molecular dynamics study. Appl. Phys. Lett. **2011**, *98*, 113107.
61. Berber, S.; Kwon, Y.-K.; Tomanek, D. Unusually high thermal conductivity in carbon nanotubes. Phys. Rev. Lett. **2000**, *84*, 4613.
62. Lindsay, L.; Broido, D.A.; Mingo, N. Flexural phonons and thermal transport in multilayer graphene and graphite. Phys. Rev. B **2011**, *83*, 235428.
63. Singh, D.; Murthy, J.Y.; Fisher, T.S. Mechanism of thermal conductivity reduction in few-layer graphene. J. Appl. Phys. **2011**, *110*, 044317.
64. Jang, W.; Chen, Z.; Bao, W.; Lau, C.N.; Dames, C. Thickness-dependent thermal conductivity of encased graphene and ultrathin graphite. Nano Lett. **2010**, *10*, 3909.
65. Evans, W.J.; Hu, L.; Keblinsky, P. Thermal conductivity of graphene ribbons from equilibrium molecular dynamics: Effect of ribbon width, edge roughness, and hydrogen termination. Appl. Phys. Lett. **2010**, *96*, 203112.
66. Munoz, E.; Lu, J.; Yakobson, B.I. Ballistic thermal conductance of graphene ribbons. Nano Lett. **2010**, *10*, 1652.
67. Savin, A.V.; Kivshar, Y.S.; Hu, B. Suppression of thermal conductivity in graphene nanoribbons with rough edges. Phys. Rev. B **2010**, *82*, 195422.
68. Maultzsch, J.; Reich, S.; Thomsen, C.; Requardt, H.; Ordejon, P. Phonon dispersion in graphite. Phys. Rev. Lett. **2004**, *92*, 075501.
69. Mohr, M.; Maultzsch, J.; Dobardzic, E.; Reich, S.; Milosevic, I.; Damnjanovic, M.; Bosak, A.; Krisch, M.; Thomsen, C. Phonon dispersion of graphite by inelastic X-ray scattering. Phys. Rev. B **2007**, *76*, 035439.
70. Mounet, N.; Marzari, N. First-principles determination of the structural, vibrational and thermodynamic properties of diamond, graphite, and derivatives. Phys. Rev. B **2005**, *71*, 205214.
71. Wirtz, L.; Rubio, A. The phonon dispersion of graphite revisited. Solid State Commun. **2004**, *131*, 141.
72. Yan, J.-A.; Ruan, W.Y.; Chou, M.Y. Phonon dispersions and vibrational properties of monolayer, bilayer, and trilayer graphene: Density-functional perturbation theory. Phys. Rev. B **2008**, *77*, 125401.

Downloaded by [University of California, Riverside Libraries] at 15:37 29 October 2014

73. Falkovsky, L.A. Symmetry constraints on phonon dispersion in graphene. Phys. Lett. A **2008**, *372*, 5189.
74. Perebeinos, V.; Tersoff, J. Valence force model for phonons in graphene and carbon nanotubes. Phys. Rev. B **2009**, *79*, 241409(R).
75. Lindsay, L.; Broido, D. Optimized Tersoff and Brenner empirical potential parameters for lattice dynamics and phonon thermal transport in carbon nanotubes and graphene. Phys. Rev. B **2010**, *81*, 205441.
76. Dubay, O.; Kresse, G. Accurate density functional calculations for the phonon dispersion relation of graphite layer and carbon nanotubes. Phys. Rev. B **2003**, *67*, 035401.
77. Wang, H.; Wang, Y.; Cao, X.; Feng, M.; Lan, G. Vibrational properties of graphene and graphene layers. J. Raman Spectrosc. **2009**, *40*, 1791.
78. Mazzamuto, F.; Saint-Martin, J.; Valentin, A.; Chassat, C.; Dollfus, P. Edge shape effect on vibrational modes in graphene nanoribbons: A numerical study. J. Appl. Phys. **2011**, *109*, 064516.
79. Tan, Z.W.; Wang, J.-S.; Gan, C.K. First-principles study of heat transport properties of graphene nanoribbons. Nano Lett. **2011**, *11*, 214.
80. Droth, M.; Burkard, G. Acoustic phonon and spin relaxation in graphene nanoribbons. Phys. Rev. B **2011**, *84*, 155404.
81. Qian, J.; Allen, M.J.; Yang, Y.; Dutta, M.; Stroscio, M.A. Quantized long-wavelength optical phonon modes in graphene nanoribbon in the elastic continuum model. Superlatt. Microstruct. **2009**, *46*, 881.
82. Nika, D.L.; Pokatilov, E.P.; Askerov, A.S.; Balandin, A.A. Phonon thermal conduction in graphene: Role of Umklapp and edge roughness scattering. Phys. Rev. B **2009**, *79*, 155413.
83. Lui, C.H.; Li, Z.; Chen, Z.; Klimov, P.V.; Brus, L.E.; Heinz, T.F. Imaging stacking order in few-layer graphene. Nano Lett. **2011**, *11*, 164.
84. Cong, C.; Yu, T.; Sato, K.; Shang, J.; Saito, R.; Dresselhaus, G.F.; Dresselhaus, M.S. Raman characterization of ABA- and ABC-stacked trilayer graphene. ACS Nano **2011**, *5*, 8760.
85. Aksamija, Z.; Knezevic, I. Lattice thermal conductivity of graphene nanoribbons: Anisotropy and edge roughness scattering. Appl. Phys. Lett. **2011**, *98*, 141919.
86. Aizawa, T.; Sounda, R.; Otani, S.; Ishizawa, Y.; Oshima, C. Bond softening in monolayer graphite formed on transition-metal carbide surfaces. Phys. Rev. B **1990**, *42*, 11469.
87. Pople, J.A.; Musgrave, J.P. A General Valence Force Field for diamond. Proc. Roy. Soc. **1962**, *A268*, 474.
88. Keating, P.N. Effect of invariance requirements on the elastic strain energy of crystals with application to the diamond structure. Phys. Rev. **1996**, *145*, 637.
89. Martin, R.M. Elastic properties of ZnS structure semiconductors. Phys. Rev. B **1970**, *1*, 4005.
90. Kim, P.; Shi, L.; Majumdar, A.; Mc Euen, P.L. Thermal transport measurement of individual multiwalled nanotubes. Phys. Rev. Lett. **2001**, *87*, 215502.
91. Lippi, A.; Livi, R. Heat conduction in two-dimensional nonlinear lattices. J. Stat. Phys. **2000**, *100*, 1147.
92. Yang, L. Finite heat conductance in a 2D disorder lattice. Phys. Rev. Lett. **2002**, *88*, 094301.
93. Dhar, A. Heat conduction in the disordered harmonic chain revisited. Phys. Rev. Lett. **2001**, *86*, 5882.
94. Casher, A.; Lebowitz, J.L. Heat flow in regular and disordered harmonic chains. J. Math. Phys. **1971**, *12*, 1701.
95. Ecsedy, D.J.; Klemens, P.G. Thermal resistivity of dielectric crystals due to 4-phonon processes and optical modes. Phys. Rev. B **1977**, *15*, 5957.
96. Mingo, N.; Broido, D. Length dependence of carbon nanotube thermal conductivity and "the problem of long waves." Nano Lett. **2005**, *5*, 1221.
97. Nika, D.L.; Askerov, A.S.; Balandin, A.A. anomalous size dependence of the thermal conductivity of graphene ribbons. Nano Lett. **2012**, *12*, 3238.
98. Lindsay, L.; Broido, D.A.; Mingo, N. Diameter dependence of carbon nanotube thermal conductivity and extension to the graphene limit. Phys. Rev. B **2010**, *82*, 161402.
99. Klemens, P.G. Theory of thermal conduction in the ceramic films. Int. J. Thermophys. **2001**, *22*, 265.
100. Nika, D.L.; Ghosh, S.; Pokatilov, E.P.; Balandin, A.A. Lattice thermal conductivity of graphene flakes: Comparison with bulk graphite. Appl. Phys. Lett. **2009**, *94*, 203103.
101. Kelly, B.T. *Physics of Graphite*; Applied Science Publishers: London, 1981.
102. Kong, B.D.; Paul, S.; Nardelli, M.B.; Kim, K.W. First-principles analysis of lattice thermal conductivity in monolayer and bilayer graphene. Phys. Rev. B **2009**, *80*, 033406.
103. Nika, D.L.; Pokatilov, E.P.; Balandin, A.A. Theoretical description of thermal transport in graphene: The issues of phonon cut-off frequencies and polarization branches. Phys. Stat. Sol. B **2011**, *248*, 2609.
104. Zhang, H.; Lee, G.; Cho, K. Thermal transport in graphene and effects of vacancies. Phys. Rev. B **2011**, *84*, 115460.
105. Wei, N.; Xu, L.; Wang, H.-Q.; Zheng, J.-C. Strain engineering of thermal conductivity in graphene sheets and nanoribbons: A demonstration of magic flexibility. Nanotechnology **2011**, *22*, 105705.
106. Hao, F.; Fang, D.; Xu, Z. Mechanical and thermal transport properties of graphene with defects. Appl. Phys. Lett. **2011**, *99*, 041901.
107. Chen, S.; Li, Q.; Zhang, Q.; Qu, Y.; Ji, H.; Ruoff, R.S.; Cai, W. Thermal conductivity measurements of suspended graphene with and without wrinkles by micro-Raman mapping. Nanotechnology **2012**, *23*, 365701.
108. Lindsay, L.; Broido, D.A.; Mingo, N. Flexural phonons and thermal transport in graphene. Phys. Rev. B **2010**, *82*, 115427.
109. Adamyan, V.; Zavalniuk, V. Lattice thermal conductivity of graphene with conventionally isotopic defects. J. Phys. Condens. Matter. **2012**, *24*, 415401.
110. Chen, L.; Kumar, S. Thermal transport in graphene supported on copper. A. J. Appl. Phys. **2012**, *112*, 043502.
111. Wei, Z.; Ni, Z.; Bi, K.; Chen, M.; Chen, Y. In-plane lattice thermal conductivities of multilayer graphene films. Carbon **2011**, *49*, 2653.
112. Nika, D.L.; Balandin, A.A. Two-dimensional phonon transport in graphene. J. Phys. Condens. Matter. **2012**, *24*, 233203.
113. Jiang, J.-W.; Wang, J.-S.; Li, B. Thermal conductance of graphite and dimerite. Phys. Rev. B **2009**, *79*, 205418.
114. Huang, Z.; Fisher, T.S.; Murthy, J.Y. Simulation of phonon transmission through graphene and graphene nanoribbons with a Green's function method. J. Appl. Phys. **2010**, *108*, 094319.

115. Hu, J.; Ruan, X.; Chen, Y.P. Thermal conductivity and thermal rectification in graphene nanoribbons: A molecular dynamic study. Nano Lett. **2009**, *9*, 2730.
116. Guo, Z.; Zhang, D.; Gong, X.-G. Thermal conductivity of graphene nanoribbons. Appl. Phys. Lett. **2009**, *95*, 163103.
117. Zhai, X.; Jin, G. Stretching-enhanced ballistic thermal conductance in graphene nanoribbons. EPL **2011**, *96*, 16002.
118. Jiang, J.-W.; Wang, B.-S.; Wang, J.-S. First principle study of the thermal conductance in graphene nanoribbon with vacancy and substitutional silicon defects. Appl. Phys. Lett. **2011**, *98*, 113114.
119. Ouyang, T.; Chen, Y.P.; Yang, K.K.; Zhong, J.X. Thermal transport of isotopic-superlattice graphene nanoribbons with zigzag edge. EPL **2009**, *88*, 28002.
120. Wang, Z.; Mingo, N. Absence of Casimir regime in two-dimensional nanoribbon phonon conduction. Appl. Phys. Lett. **2011**, *99*, 101903.
121. Hu, J.; Wang, Y.; Vallabhaneni, A.; Ruan, X.; Chen, Y. Nonlinear thermal transport and negative differential thermal conductance in graphene nanoribbons. Appl. Phys. Lett. **2011**, *99*, 113101.
122. Xie, Z.-X.; Chen, K.-Q.; Duan, W. Thermal transport by phonons in zigzag graphene nanoribbons with structural defects. J. Phys. Condens. Matter. **2011**, *23*, 315302.
123. Murali, R.; Yang, Y.; Brenner, K.; Beck, T.; Meindl, J.D. Breakdown current density of graphene nanoribbons. Appl. Phys. Lett. **2009**, *94*, 243114.
124. Liao, A.D.; Wu, J.Z.; Wang, X.; Tahy, K.; Jena, D.; Dai, H.; Pop, E. Thermally limited current carrying ability of graphene nanoribbons. Phys. Rev. Lett. **2011**, *106*, 256801.
125. Wang, Y.; Qiu, B.; Ruan, X. Edge effect on thermal transport in graphene nanoribbons: A phonon localization mechanism beyond edge roughness scattering. Appl. Phys. Lett. **2012**, *101*, 013101.

Graphene–Guests
Downloaded by [University of California, Riverside Libraries] at 15:37 29 October 2014